www.sciencemag.org/cgi/content/full/science.aar4142/DC1

Supplementary Material for

Plants send small RNAs in extracellular vesicles to fungal pathogen to silence virulence genes

Qiang Cai, Lulu Qiao, Ming Wang, Baoye He, Feng-Mao Lin, Jared Palmquist, Hsien-Da Huang, Hailing Jin*

*Corresponding author. Email: hailingj@ucr.edu

Published 17 May 2018 as *Science* First Release
DOI: 10.1126/science.aar4142

This PDF file includes:

Materials and Methods
Supplementary Text
Fig. S1 to S16
References

Other Supplementary Material for this manuscript includes the following:
(available at www.sciencemag.org/content/science.aar4142/DC1)

Tables S1 to S6 as separate Excel files

Materials and Methods

Materials

Arabidopsis thaliana ecotype *Col-0* and *Nicotiana benthamiana* were used in this study. *Arabidopsis* mutants *tet8* (Salk_136039c), *dcl2-1dcl3-1dcl4-2* (*dcl2/3/4*), *rdr6-15*, and marker lines $TET8_{pro}$*::TET8-GFP* and $35S_{pro}$*::ARA6-GFP* were described previously (*17, 29-31*).

The *B. cinerea* strain B05.10 was used in this study.

Constructs for expressing CFP or YFP-tagged *ARA6, TET8, TET9*, and YFP-tagged fungal target genes were generated using pEarleyGate binary vectors.

For complementation analysis, the *TET8* coding sequence was fused with a CFP tag under the Cauliflower Mosaic Virus 35S promoter in a pEarleyGate binary vector. The construct was introduced into the *tet8* mutant background to generate the complementation lines.

For CRISPR/Cas9-mediated gene editing of *TET9*, designed guide RNAs were expressed under the U6 promoter (*32*). The GEX1 ovule specific promoter was used to drive Cas9 expression in this vector. The designed guide RNA sequences are listed in table S6.

The *tet8 tet9* double mutant lines were generated via *TET9* knock-down (35S:amiRNA-*TET9*) in the *tet8* mutant background.

Artificial miRNA constructs were generated using the miR319a backbone (pRS300 plasmid) (*33*) for sRNA overexpression lines (TAS1c-siR483 ox and TAS2-siR453 ox) in the wild-type *Col-0* background.

The short tandem target mimic (STTM)-TAS1/2 construct used to inactivate both TAS1c-siR483 and TAS2-siR453 was generated according to the procedure by Tang and colleagues (*34*). Briefly, the sub-cloning vector was amplified and the Poly-Cis site was replaced by the STTM structure used for targeting both TAS1c-siR483 and TAS2-siR453. The PCR product that includes the pOT2 backbone (−3.6 kb) was purified and cleaved by SwaI, followed by purification and self-ligation. The recombinant plasmid was then introduced into a modified pFGC5941 binary vector through the unique *PacI* site. This strategy is the same as what we used to generate STTM-miR825 lines previously to knock down both miR825 and miR825* (*35*).

Arabidopsis plants were transformed using the floral dip method with *Agrobacterium tumefaciens* strain GV3101 carrying the corresponding cloned binary vectors.

Transient co-expression assays in *Nicotiana benthamiana* were performed by infiltrating 3-week-old *N. benthamiana* plants with *Agrobacterium* (OD600 =1.0).

For generating *B. cinerea* target gene knockout mutants, we used a homologous recombination-based method to knock out *B. cinerea* genes described previously (*36*).

All primers are listed in table S6.

Methods

Fungal pathogen assays

The *B. cinerea* spores were diluted in 1% sabouraud maltose broth buffer to a final concentration of 10^5 spores/ml for drop inoculation of four-week-old *Arabidopsis* plants (*8*). The lesion sizes of *B. cinerea*-infected plant materials were measured and calculated using ImageJ software.

Isolation of pure fungal cells from infected plant leaves

B. cinerea protoplasts were purified from infected *Arabidopsis* leaves using a method that takes advantage of the differences between plant and fungal cell wall components (*37*, *38*). After rinsing with sterilized water to remove ungerminated fungal spores, the leaves were homogenized for 1 minute in isolation buffer (0.02 M MOPS buffer pH 7.2, 0.2 M sucrose) in a blender using the highest speed setting to release fungal cells from host epidermal cells. The homogenate was then filtered through 70 μm nylon mesh to remove plant cell wall debris. After the filtrate was collected, material retained on the filter was re-homogenized in isolation buffer for 1 minute, and re-filtered. After centrifuging the pooled homogenate at 1,500 g for 10 minutes, the pellets were re-suspended in 1% Triton X-100 and washed 3 times with isolation buffer to remove some plant contents. The pellets were then processed for plant cell wall digestion using plant cell wall digest solution (1.5% cellulose, 0.4% maceroenzyme, 0.4 M mannitol, 20 mM MES (pH 5.7), 20 mM KCl, $CaCl_2$, 0.1% BSA) as described previously (*39*), followed by resuspension in 1% Triton X-100 and washing in isolation buffer 5 times to completely remove plant contents. After centrifugation at 1,500 g for 10 minutes, the pellets were re-suspended in lysing enzyme solution (2% lysing enzyme from *Trichoderma harzianum* (Sigma) in 0.6 M KCl, 50 mM $CaCl_2$) and incubated for 2-3 hours at 28^{o}C to release fungal protoplasts. The fungal protoplasts were filtered through a 40 μm nylon mesh, and gently overlaid with a 30% sucrose solution to form a distinct interface with the fungal tissue suspension and centrifuged at 4°C for 10 minutes at 5,000 rpm. The fungal protoplasts were collected from the interface of the sucrose layer and the tissue suspension layer. The sucrose was removed from the purified protoplast solution by diluting five- to ten-fold with SM buffer (1.2 M-sorbitol and 0.02 M-MES, pH 6.0) and centrifuging at 5,000 rpm for 5 minutes. Repeating the sucrose density gradient centrifugation step can increase the purity. After completely removing the supernatant, the pellet was resuspended in Trizol Reagent (Invitrogen) for RNA extraction. As a control, cultured *B.cinerea* was mixed with un-infected leaves subjected to the same procedure as *B.cinerea* protoplast isolated from *Arabidopsis* leaves infected with *B.cinerea*.

Extracellular vesicle isolation

Plant extracellular vesicles were isolated from apoplastic fluids and purified by differential ultracentrifugation (*40, 41*). The apoplastic fluids were extracted from *Arabidopsis* leaves by vacuum infiltration with infiltration buffer (20 mM MES, 2 mM $CaCl_2$, 0.1 M NaCl, pH 6.0), then with low spinning at 900 g to collect the apoplastic fluids. Before purification of vesicles, cellular debris was removed by spinning at 2,000 g for 30 minutes and filtering the apoplastic fluids through a 0.45 μm filter and then spun at 10,000 g for 30 minutes. Because the pellet from 100,000 *g* centrifugation has been established to contain extracellular vesicles (*42*), the final supernatant was spun at 100,000 g for 1 hour and the pelleted material was washed with filtered infiltration buffer at 100,000 g for 1 hour to collect the pellet.

sRNA cloning and illumina HiSeq data analysis

The sRNA libraries were made using Illumina TruSeq® Small RNA Sample Prep Kits and sequenced on an Illumina HiSeq system. The sRNA sequencing reads were preprocessed with the procedure of quality control and adapter trimming by using fastxtoolkit (http://hannonlab.cshl.edu/fastx_toolkit/index.html). The sequences were mapped to *Arabidopsis* (TAIR10) or *B. cinerea* B05.10 genomes and only the reads that matched perfectly to each genome were used for further analysis. After removal of tRNA-, rRNA-, snoRNA-, and snRNA-mapped reads, the read numbers of sRNA in each library were normalized by the total number of sRNA reads, resulting in reads per million (RPM) normalized measurements. The sRNAs listed in the supplementary tables S1-S5 were detected in all three biological repeats. For purified *B. cinerea* cell libraries and extracellular vesicles libraries, 40 normalized reads per million (RPM) sRNA reads were used as a cutoff. Total *Arabidopsis* sRNA libraries were used as a reference control. In purified *B. cinerea* cell libraries, the normalized reads number of selected sRNAs must be 10 times higher than that in the control libraries. The *B. cinerea* target gene prediction for *Arabidopsis* sRNAs was performed as previously described (*6*).

sRNA and gene expression analyses

RNA was extracted using the Trizol extraction method. Purified RNA was treated with DNase I then first strand cDNA was synthesized using the Superscript III kit (Invitrogen, CA). sRNA RT-PCR was performed as previously described (*6*). Quantitative PCR was performed with the CFX384 real-time PCR detection system (Bio-Rad) using the SYBR Green mix (Bio-Rad).

For determining if sRNAs were localized within vesicles, purified vesicles were treated with 10 U of micrococcal nuclease (MNase)(Thermo Fisher) with or without Triton-X-100. For Triton-X-100 treatment, vesicles were incubated with 1% Triton-X-100 on ice

for 30 minutes before nuclease treatments. Nuclease treatment was carried out at 37°C for 15 minutes followed by RNA isolation. Levels of sRNAs in *B. cinerea* cells was determined by ligation-based sRNA RT-PCR, which was described previously (*11*). Primer sequences are provided in table S6.

5′- RNA-linker-mediated RACE assay to detect mRNA cleavage products

For the 5′-RNA-linker-mediated RACE assay, total RNA was extracted from *B. cinerea*-infected *Arabidopsis* and directly ligated to the 5'-RNA adapter without further modification. cDNA was synthesized with reverse transcriptase using Oligo (dT) primers or gene specific primers. Gene-specific 5′-RACE PCR amplifications were done with the 5′ Nested Primer and gene-specific primers. The PCR fragments obtained from 5' RACE was inserted into the pGEM18-T easy vector (Promega), and 10-15 individual clones were selected for DNA sequencing. All primer sequences are listed in table S6.

Confocal microscopy analyses

Following the protocol of visualization of membranes and extracellular vesicles in plants (*43*), short staining by lipophilic dye FM4-64 was used to visualize membrane structures, such as the plasma membrane and extracellular vesicles outside of plant cells (*43*). Briefly, leaves were infiltrated with 10 μM FM4-64 dye for 30 minutes before examination. Samples were imaged using a 40x water immersion dip-in lens mounted on a Leica TCS SP5 confocal microscope (Leica Microsystems). Fluorescence intensity measurements were done using the Leica SP5 software. Lines were drawn to determine a region of interest (ROI) and fluorescence intensity was determined per pixel along the ROI.

For visualization of exosome-associated GFP-fluorescence in ultracentrifuge fractions, suspended pellets were examined using a 40x water immersion or dip-in lens mounted on a Leica TCS SP5 confocal microscope. For visualization of exosome uptake, purified exosomes were incubated with germinated *B. cinerea* at room temperature for 2 hours following confocal analyses. For Triton-X-100 treatment, the incubated fungal cells were washed with 1% Triton-X-100 for 15 minutes to remove nonspecific associations.

Transmission electron microscopy analysis

At 12 hpi of *B. cinerea*, 2-to 3-mm^2 of *Arabidopsis* leaves were fixed with 2% (v/v) glutaraldehyde in 0.1 M cacodylate buffer, pH 7.2, for 12 h at 4°C. Then the samples were rinsed with cacodylate buffer and fixed in 1% (w/v) osmium tetroxide before dehydration in ethanol with a graded series of concentrations and embedment in Epon 812 resin. Ultrathin sections were collected on 200-mesh nickel grids coated with

Formvar and stained with uranyl acetate and lead citrate. Sections were examined with a Tecnai12 TEM transmission electron microscope at an accelerating voltage of 80 kV.

Co-immunoprecipitation assay

Total protein was extracted from *N. benthamiana* leaves expressing *TET8-FLAG* and/or *TET9-GFP* using extraction buffer (50 mM Tris–HCl at pH 7.5, 150 mM NaCl, 10% glycerol, 1 mM DTT, 1 mM EDTA, 1% NP40, proteinase inhibitor cocktail; Sigma) 3 days post Agrobacterial infiltration. After shaking for 1 hour at 4 ^{o}C, cell debris was removed by centrifugation at 16,000 g for 30 min. The supernatants were incubated with Anti-FLAG M2 affinity gel (Sigma) for 4-8 hours at 4°C. The immunoprecipitation complexes were washed three times in phosphate-buffered saline (PBS: 0.1M NaCl, 90mM sodium phosphate, pH 7.0). The FLAG- or GFP-tagged proteins were detected by Western blot using anti-FLAG (Sigma) and anti-GFP antibodies (Roche), respectively. The reciprocal co-immunoprecipitation of TET9-FLAG and/or TET8-GFP was performed in the same way.

Supplementary figures

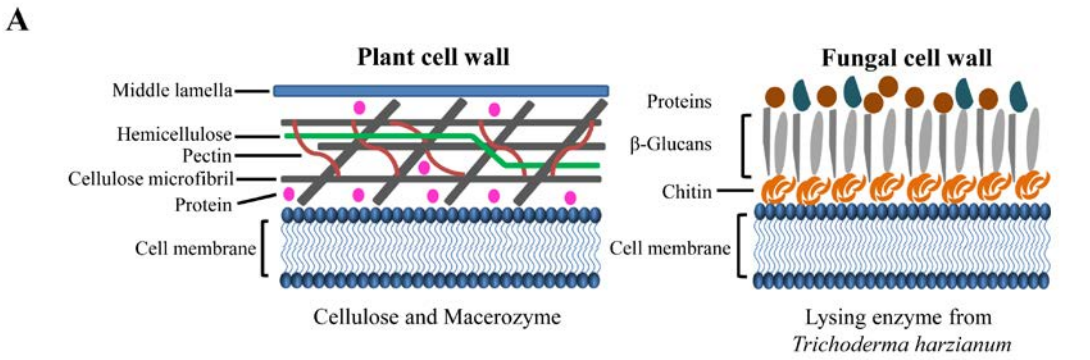

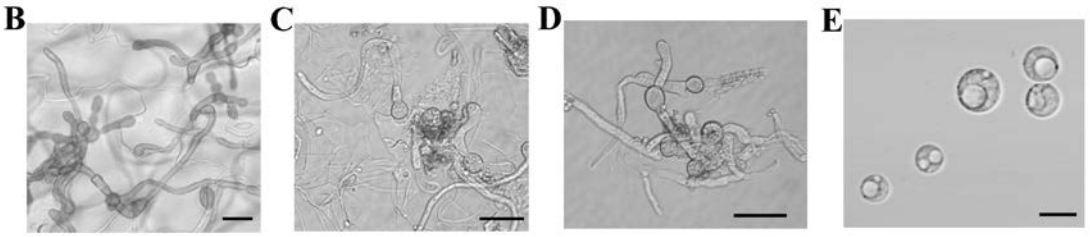

F

	Total mock	Total *Bc*-infected	Bc^{Ctrl}	Bc^{Col}
At-UBQ5	19.37±0.09	19.65±0.15	No Ct	No Ct
At-ASK	19.66±0.12	19.97±0.11	No Ct	No Ct
Bc-ITS	No Ct	21.25±0.87	18.51±0.51	18.65±0.54

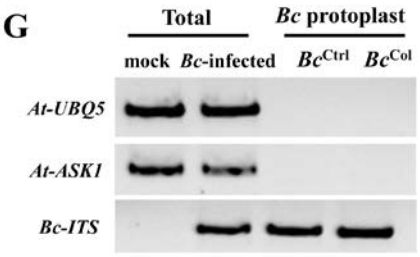

Fig. S1. Isolation of pure *B. cinerea* cells from infected *Arabidopsis* tissue using the sequential protoplast purification method. (A) Representation of plant and fungal cell walls. Plant cell walls, mainly composed of cellulose, hemicellulose, pectin, and proteins, can be digested by cellulose and macerozyme. Fungal cell walls, mainly composed of chitin, glucans, and proteins, can be digested by lysing enzyme from *Trichoderma harzianum*. (B-E) Microscopic images show the various steps in fungal protoplast isolation from infected *Arabidopsis: B. cinerea* on infected *Arabidopsis* leaves (B), mixed cells isolated from *B. cinerea*-infected leaves (C), *B. cinerea* cells after breaking plant protoplasts (D), and purified *B. cinerea* protoplasts isolated from *Arabidopsis* leaves (E). Scale bars, 20 μm. (F-G) Genomic DNA of *Botrytis* and *Arabidopsis* was measured by quantitative PCR (F) and semi-quantitative PCR (G) analysis of *Bc-ITS*, *At-UBQ5* and *At-ASK* from the purified fungal protoplasts. In (F), the Ct value of each gene is shown in the table.

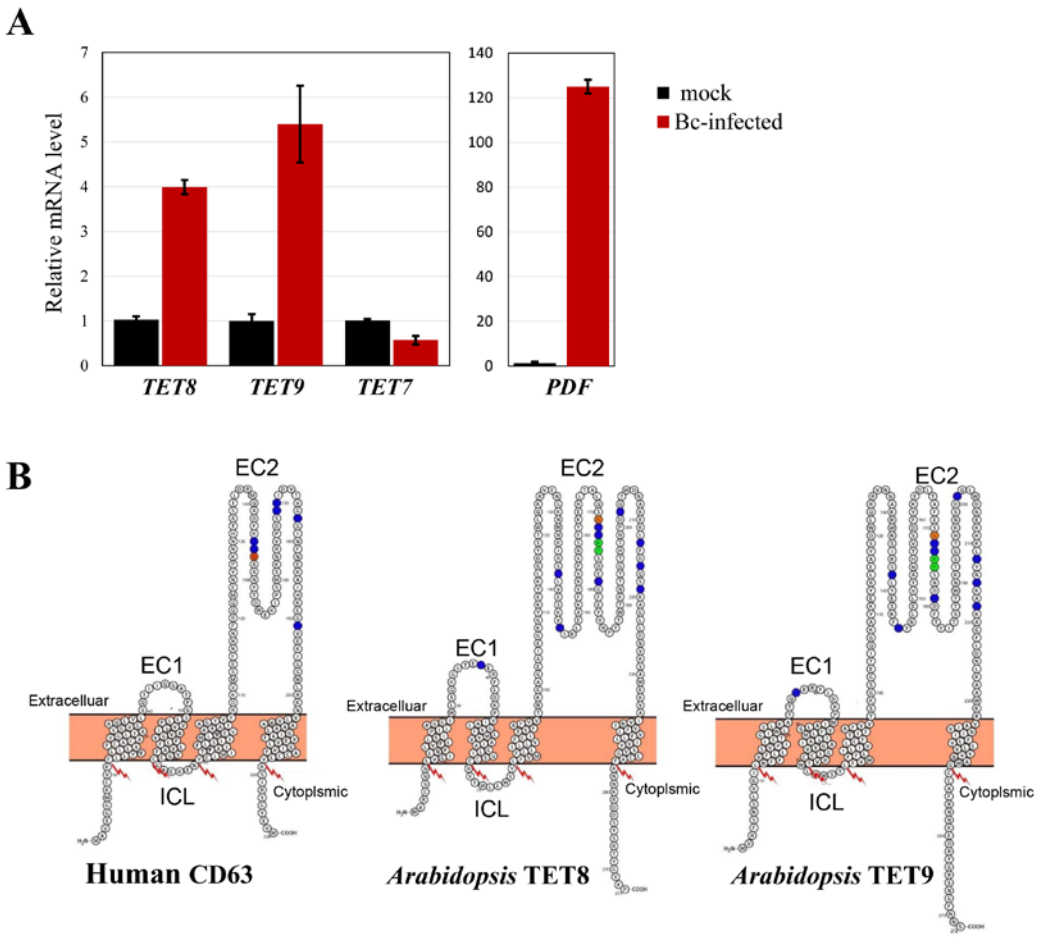

Fig. S2. Expression and structural analysis of TET8 and TET9. (A) Expression levels of *TET8* and *TET9* were induced by *B. cinerea* infection. *TET7* and *PDF1.2* were used as controls. Expression of *At-UBQ* was used as an internal control. Error bars indicate the standard deviation of three technical repeats. Similar results were obtained from three biological replicates. (B) The predicted structures and the topology of plant tetraspanins TET8 and TET9 are similar to that of human CD63**.** Images were made using Protter (http://molbiol-tools.ca/Protein_secondary_ structure.htm). Conserved cysteines from the plant GCCK/RP motif and animal CCG motif in EC2 (large extracellular domain) are marked. In plants, a conserved cysteine in EC1 (small extracellular domain) is also marked. Potential palmitoylation sites in transmembrane domains are indicated with red zigzag lines.

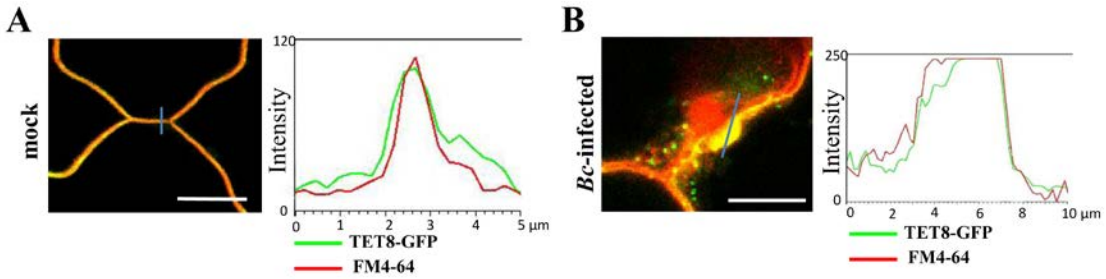

Fig. S3. Fluorescence intensity quantification of the images in Fig.2A. TET8-GFP localization was measured under mock treatment (A) and after *B. cinerea* infection (B). Transections used for fluorescence intensity measurements are indicated by blue lines. Green and red lines indicate TET8-GFP and FM4-64 fluorescent intensities, respectively. Scale bars, 10 µm.

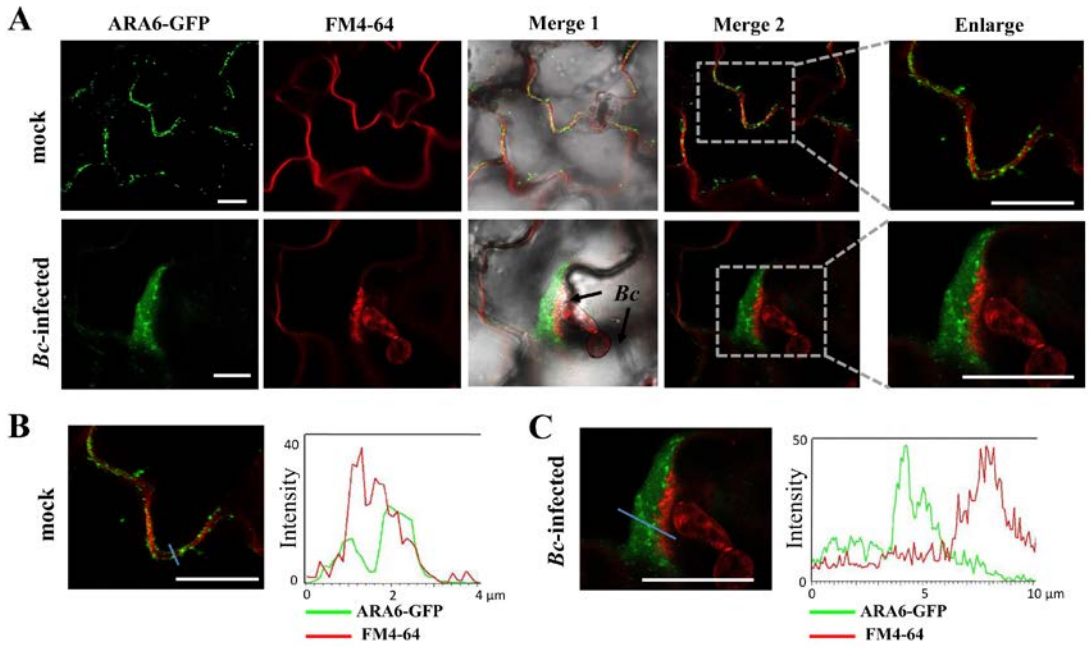

Fig. S4. *B. cinerea* induces ARA6 accumulation at the site of fungal infection. (A) *B. cinerea* infected *Arabidopsis* leaves expressing *ARA6-GFP* were examined at 12 hpi. Short staining of FM4-64 was applied 30 minutes before examination to stain extracellular vesicles and plasma membranes. ARA6-labeled vesicles accumulate near the fungal infection sites (*Bc* with black arrows), and do not co-localize with FM4-64-labeled extracellular vesicles. (B-C) The fluorescence intensity of the images in (A) was quantified. Transections used for fluorescence intensity measurements are indicated by blue lines. Green and red lines represent histograms of ARA6-GFP and FM4-64 fluorescent intensities, respectively. Scale bars, 10 μm.

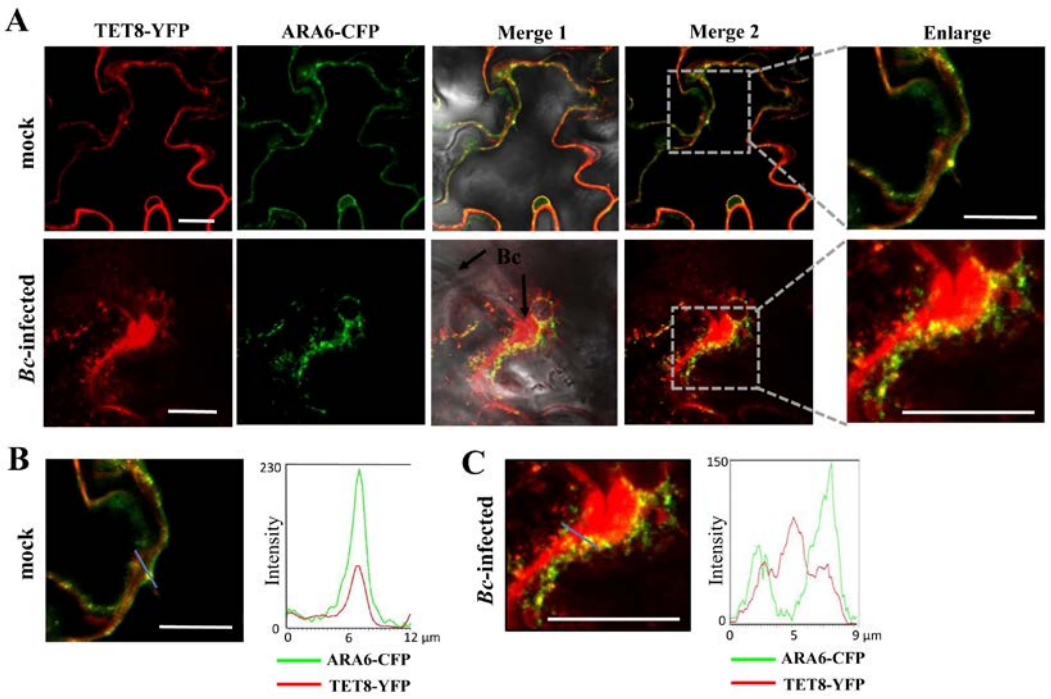

Fig. S5. Partial co-localization of ARA6 and TET8. (A) Co-expression of TET8-YFP and ARA6-CFP was examined at 12 hpi of *B. cinerea*. ARA6- and TET8-labeled vesicles partly co-localize near the fungal infection site (*Bc* with black arrows). (B-C) Fluorescent intensity was quantified for the images used in (A). Transections used for fluorescence intensity measurements are indicated by blue lines. Green and red lines represent histograms of ARA6-CFP and TET8-YFP fluorescent intensities, respectively. Scale bars, 10 μm.

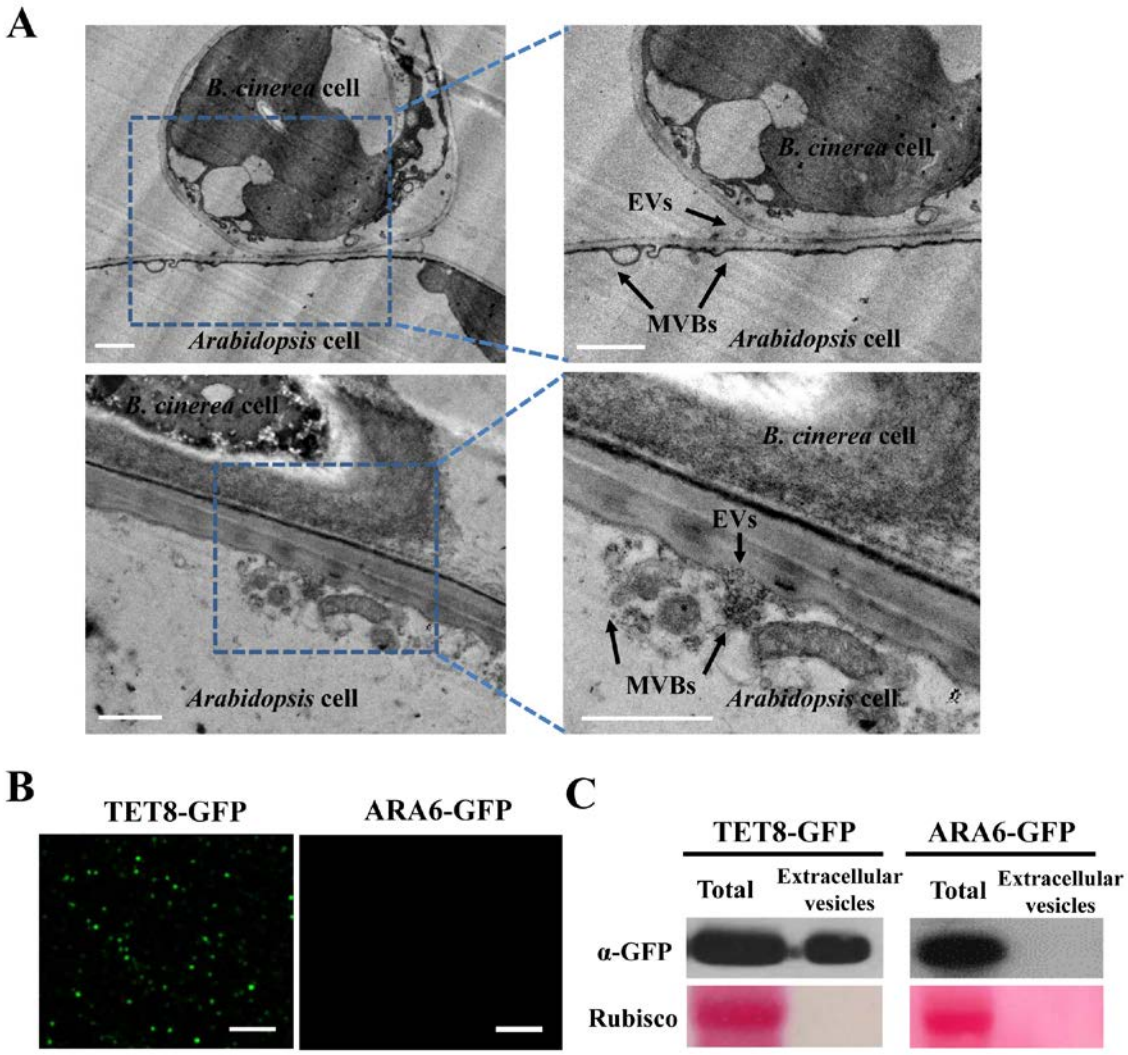

Fig. S6. ***Arabidopsis*** **cells secrete TET8-associated extracellular vesicles during the** ***B. cinerea*** **infection.** (A) Transmission electron microscopic images of plant MVBs fusing with plasma membrane to release EVs at the fungal infection sites. EVs, Extracelluar vesicles; MVBs, Multivesicular Bodies. Scale bars, 1μm. (B) TET8-GFP-associated vesicles are present in the apoplastic fractions. The MVB marker ARA6-GFP was used as a negative control. Scale bars, 10 μm. (C)GFP-labeled TET8, but not ARA6, accumulates in the extracellular vesicle fractions. The 'total' lanes indicate total protein extracts from whole leaves. Rubisco is shown as a loading control.

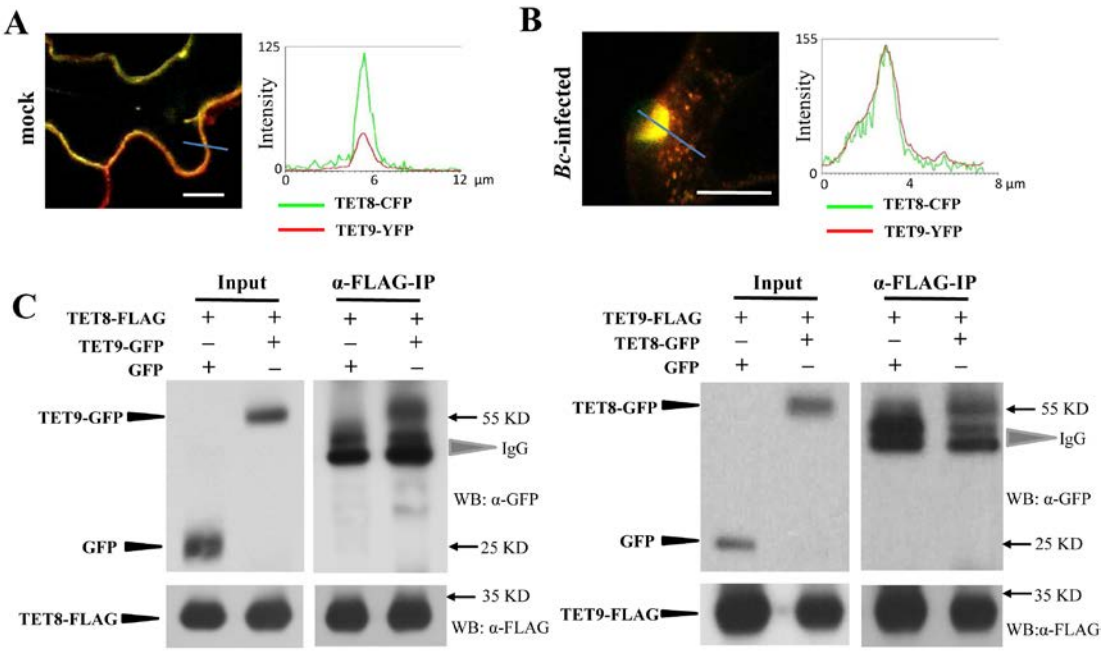

Fig. S7. TET8 is associated with TET9. (A-B) Fluorescence intensity quantification of images presented in Fig.3A. Transections used for fluorescence intensity measurements are indicated by blue lines. Green and red lines represent histograms of TET8-CFP and TET9-YFP fluorescent intensities, respectively. Scale bars, 10 μm. (C) TET8 was co-immunoprecipitated with TET9 when TET8 was pulled down using anti-FLAG M2 affinity gel, and TET9-GFP was detected by western blot using anti-GFP antibody (left panel). The reciprocal coimmunoprecipitation of TET9-FLAG and TET8-GFP confirmed the binding of TET8 and TET9 (right panel).

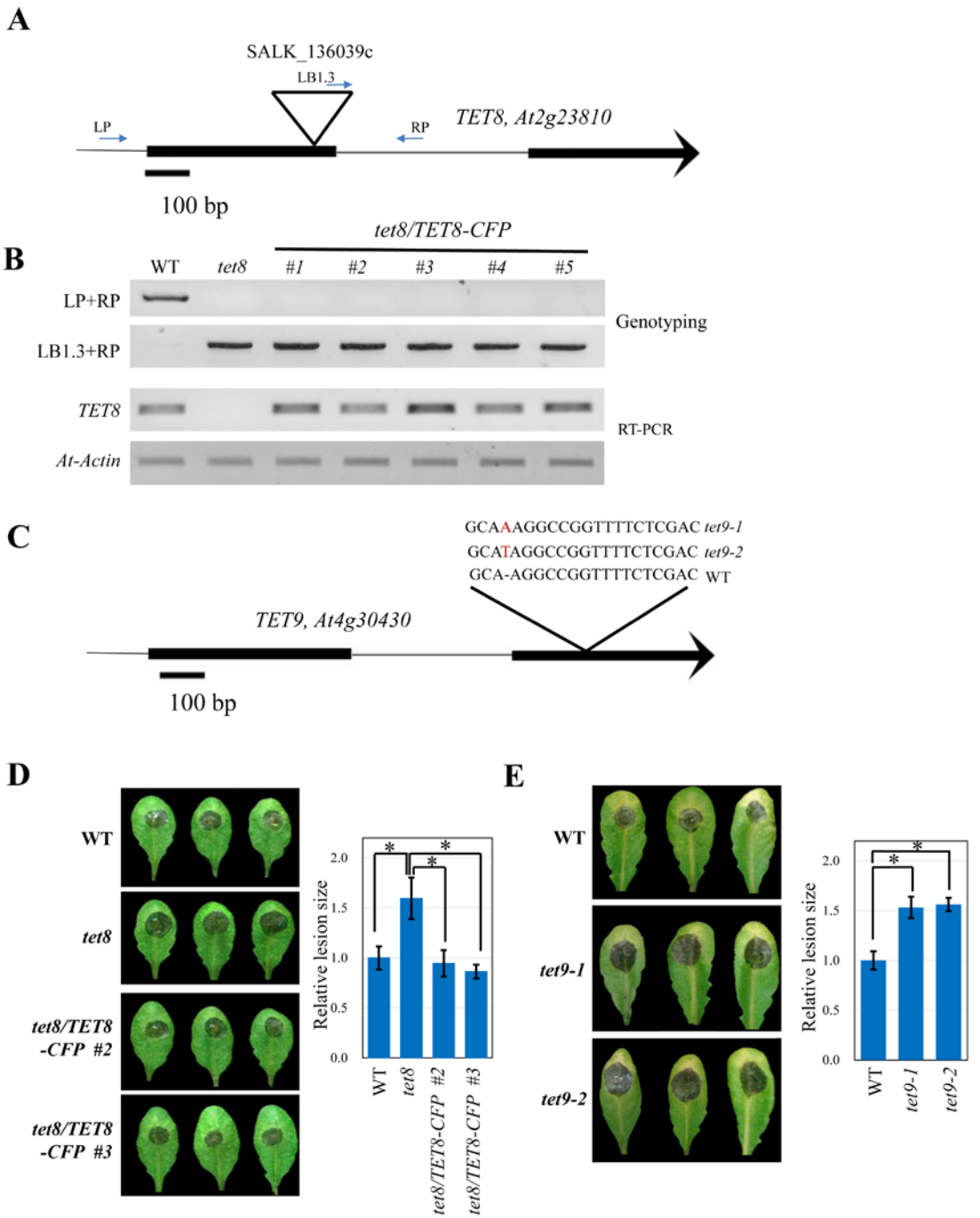

Fig. S8. The *tet8* and *tet9* single mutants are more susceptible to *B. cinerea* infection. (A) Schematic representation of the T-DNA insertion site within the *tet8* mutants. The LP primer and RP primer located in *TET8* promoter and intron region, respectively. The LB1.3 primer within the T-DNA insertion allows confirmation of the insertion when used with the RP primer. (B) Genotyping of the *tet8* mutant and RT-PCR analysis of *TET8* mRNA levels in the *tet8* mutant and *35S$_{pro}$:TET8-CFP/tet8* complementary lines. *At-Actin* was used as a control. Line #2 and #3 were selected for further pathogen assays. (C) CRISPR Cas9-mutagenized DNA sequences of *TET9* in the *tet9* mutants. Both *tet9-*

1 and *tet9-2* are frameshift mutants with single nucleotide insertions. (D) The *tet8* mutant is more susceptible to *B. cinerea* infection when compared with WT and the *tet8/TET8-CFP* complementary lines. (E) Both *tet9* mutants are more susceptible to *B. cinerea* infection. In (D-E), the relative lesion sizes were measured 2.5 dpi using ImageJ. error bars indicate the standard deviation of more than 10 leaves. Asterisks indicate significant difference determined by ANOVA Dunnett's multiple comparisons test ($P < 0.01$).

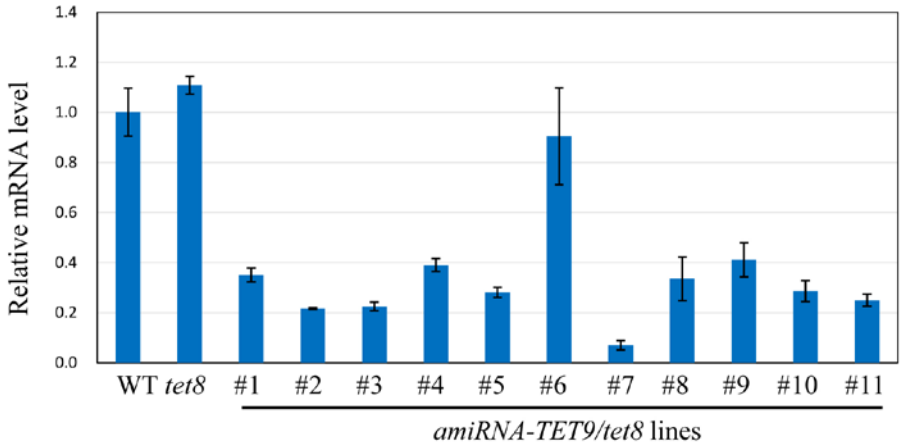

Fig. S9. Characterization of the *tet8tet9* double mutant lines. The *tet8tet9* double mutants were generated by knocking down *TET9* expression with artificial miRNA in the *tet8* background. *TET9* transcript levels were measured in 4-week-old *tet8* mutants expressing a *TET9* artificial miRNA construct and in control plant lines (wild-type [WT], and *tet8* mutant). Quantitative RT-PCR measurements were normalized to *Arabidopsis Actin* mRNA levels. Line #1 and #7 were selected for the experiments presented in Fig. 3 of this study.

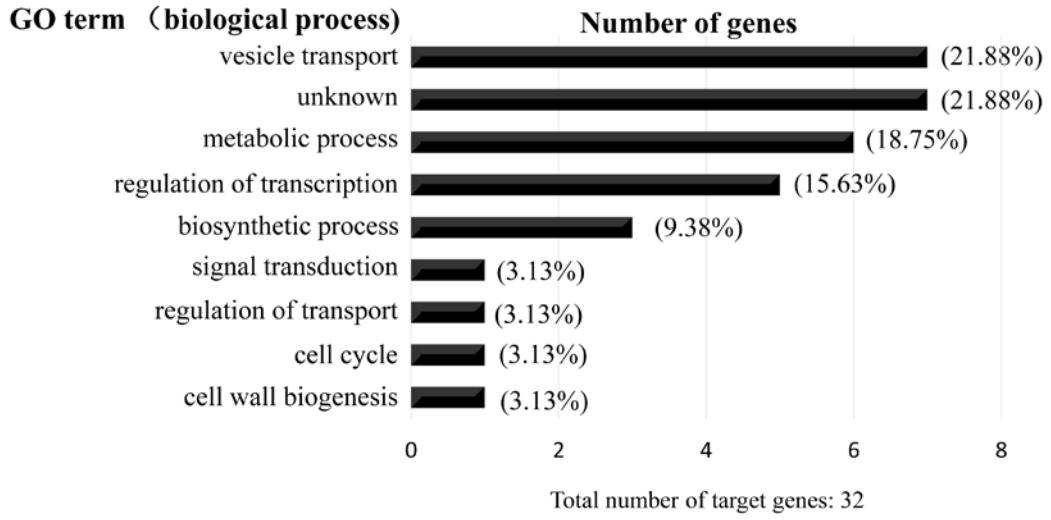

Fig. S10. Gene Ontology (GO) enrichment analysis of *B. cinerea* predicted target genes.

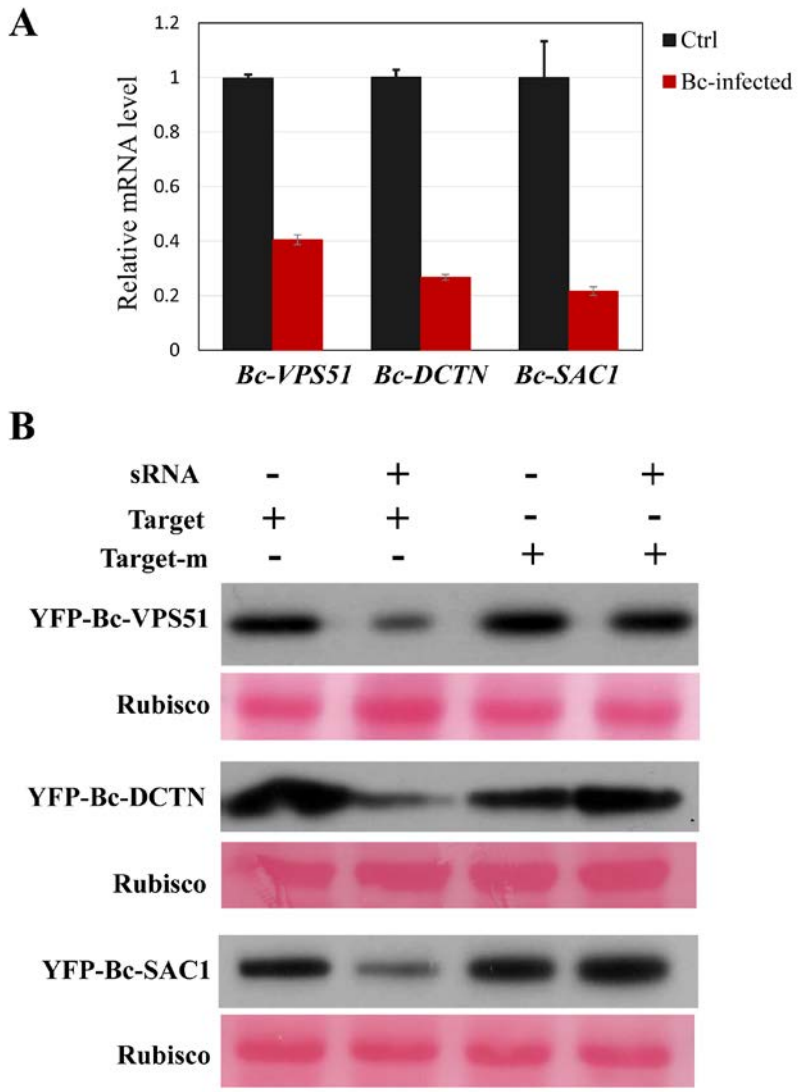

Fig. S11. *Arabidopsis* sRNAs silence *B. cinerea* target genes during infection. (A) The expression of *B. cinerea* target genes of TAS1c-siR483 and TAS2-siR453 was reduced in *B. cinerea* isolated from infected *Arabidopsis* leaves as compared with *B. cinerea* grown on medium. Expression of *Bc-Actin* was used as the internal control. Error bars indicate the standard deviation of three technical replicates. Similar results were obtained from three biological replicates. (B) Co-expression of TAS1c-siR483 and TAS2-siR453 with their YFP-tagged fungal target genes heterologously expressed in *N. benthamiana* revealed specific target silencing through Western blot analysis. The silencing effect was abolished when sRNA target sites carried synonymous mutations in the target genes (target-m). Rubisco is shown as a loading control.

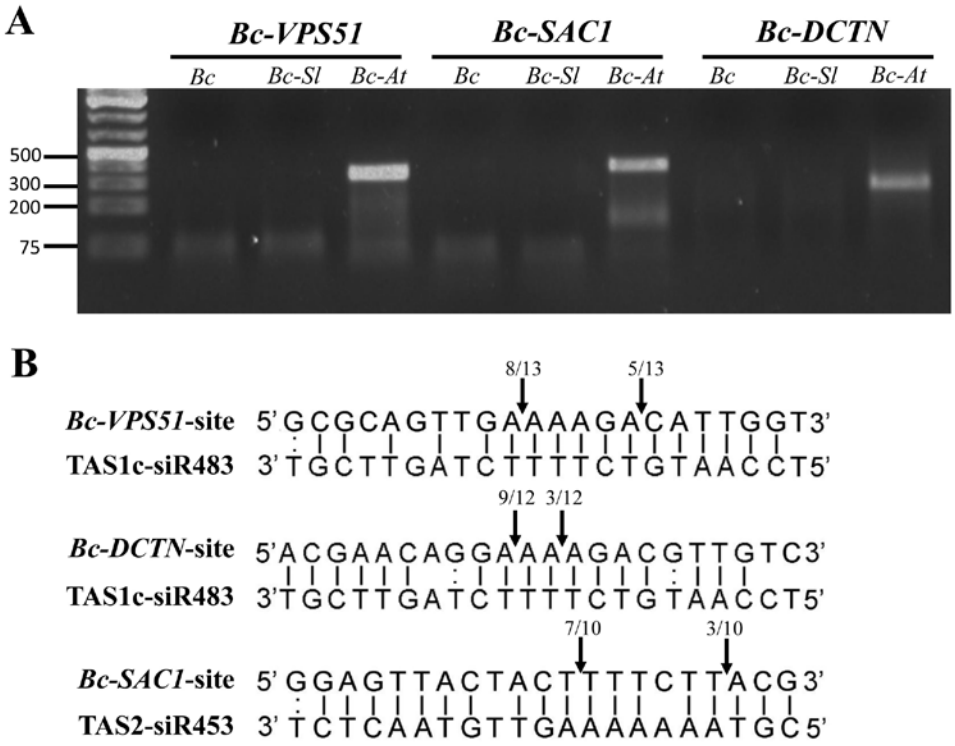

Fig. S12. Host TAS1c-siR483 and TAS2-siR453 direct mRNA cleavage of *B. cinerea* targets. (A) Nested PCR of 5′-RNAlinker-mediated RACE amplicons detected the cleavage products of *Bc-VPS51*, *Bc-SAC1* and *Bc-DCTN*, with expected sizes, from *B. cinerea* collected from infected *Arabidopsis* (*Bc-At*), but not from infected *Solanum lycopersicum* (*Bc-Sl*) or cultured *B. cinerea* (*Bc*). (B) The target cleavage sites detected in the 5'RACE assays were marked by the arrows. The number of clones corresponding to the distinct cleavage sites are marked on the top of the arrows.

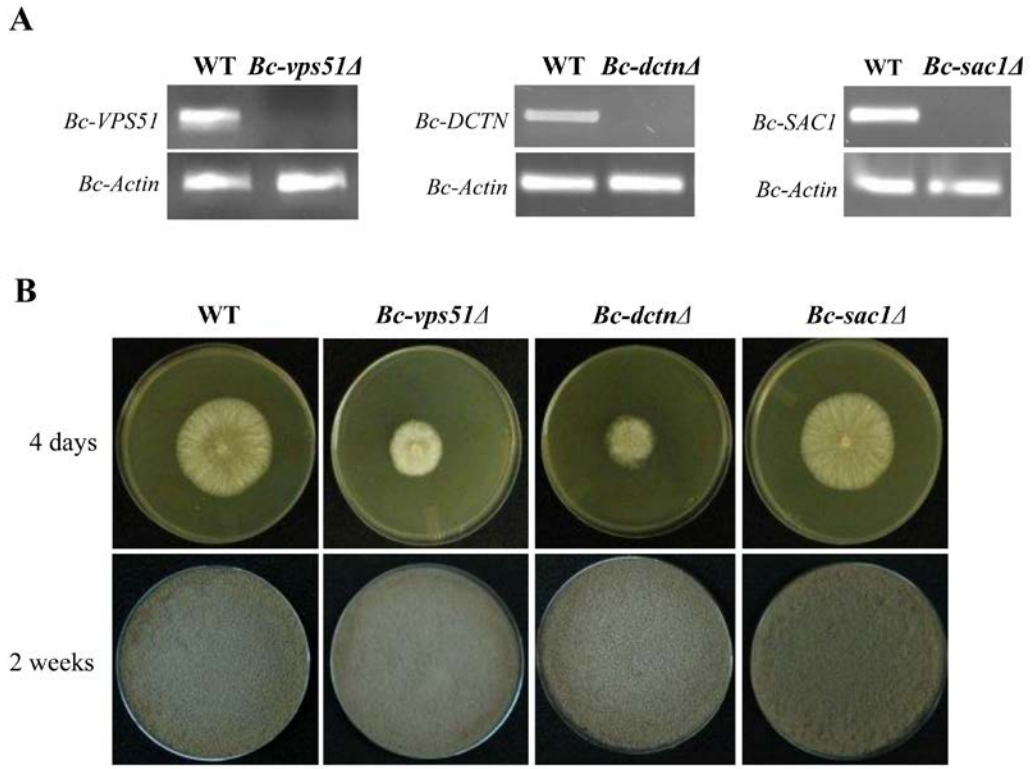

Fig. S13. The deletion mutant strains of *B. cinerea vps51Δ*, *dcnt1Δ* and *sac1Δ* were generated by homologous recombination. (A) Expression levels of each gene in corresponding mutant lines were measured by RT-PCR. The *Actin* gene of *B. cinerea* was used as an internal control. (B) The *Bc-sac1Δ* mutant did not show obvious growth defects on media, whereas the *Bc-vps51Δ* and *Bc-dcnt1Δ* mutants showed obvious reduced growth.

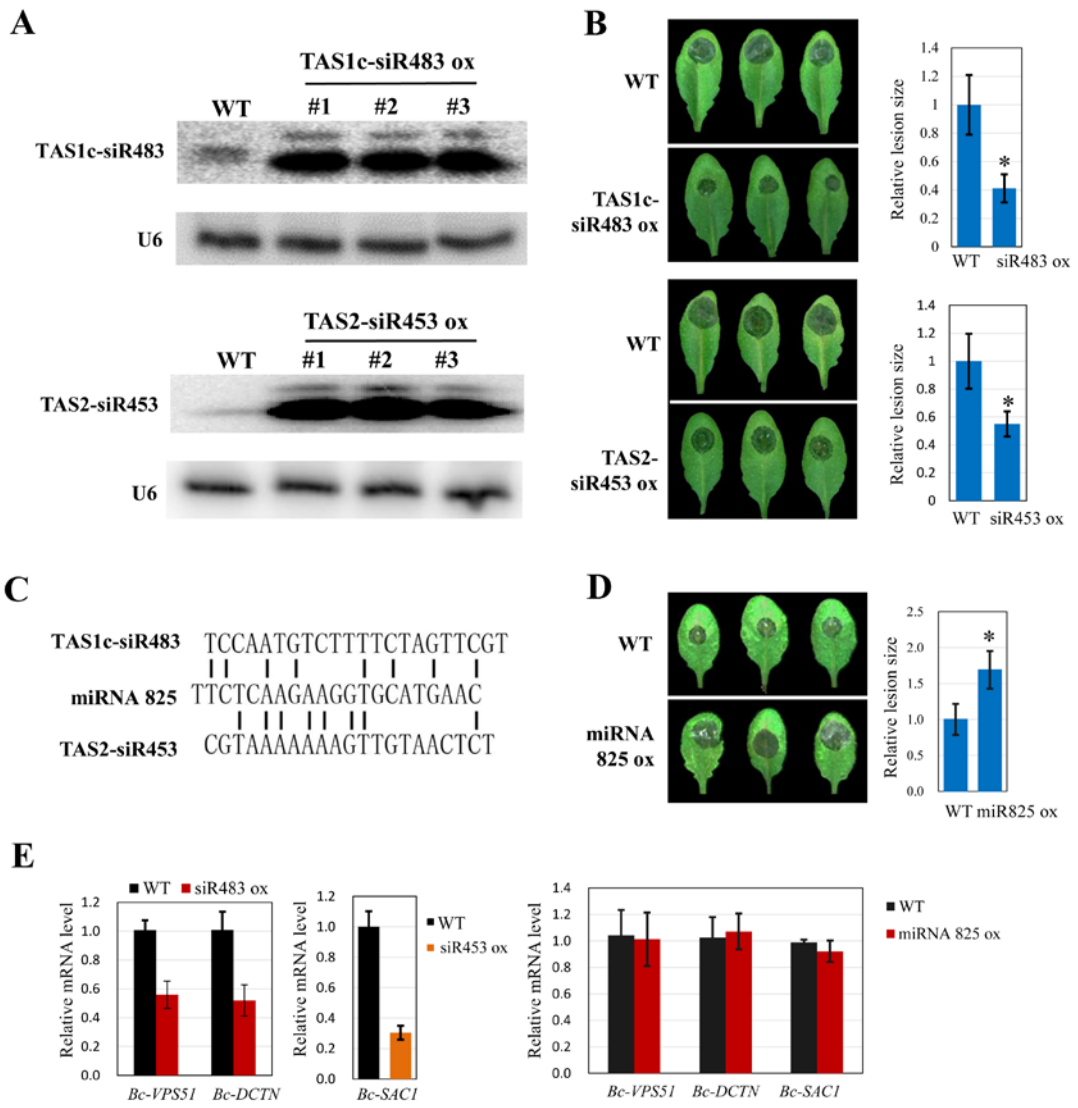

Fig. S14. Transgenic plants overexpressing transferred tasiRNAs exhibit decreased disease susceptibility to *B. cinerea* as compared with wild type. (A) Expression of TAS1c-siR483 and TAS2-siR453 in overexpression *Arabidopsis* lines was examined by Northern blot analysis. U6 was used as a loading control. Lines with high tasiRNA expression were selected for further experiments. (B) TAS1c-siR483ox and TAS2-siR453 ox plants are less susceptible to *B. cinerea* infection when compared with wild-type plants. Relative lesion sizes were measured at 3 dpi using ImageJ. (C) miR825, an sRNA with different sequence to these two tasiRNAs. (D) Transgenic plants overexpressing an unrelated sRNA, miR825, showed enhanced susceptibility to *B. cinerea* infection when compared with wild-type plants, indicating that the enhanced resistance phenotype observed in (B) is not due to overexpression of any sRNAs, but rather specific to overexpression of TAS1c-siR483 and TAS2-siR453. All the three sRNAs were expressed using the same miR319 backbone. Relative lesion sizes were measured at 2 dpi using ImageJ. In (B) and (D), error bars indicate the standard

deviation of more than 10 leaves. Asterisks indicate significant differences (two-tailed t-test, $P < 0.01$). (E) Quantitative RT-PCR results showed that *Bc-VPS51* and *Bc-DCTN1* were suppressed in *B. cinerea* from the infected TAS1c-siR483 ox plants compared to the wild type, and *Bc-SAC1* was suppressed in *B. cinerea* from infected TAS2-siR453ox plants compared to the wild type. The expression of those target genes showed no obviously difference in *B. cinerea* collected from infected miRNA825 ox plants compared to *B. cinerea* collected from infected wild type plants. The *Actin* gene of *B. cinerea* was used as an internal control. Error bars indicate the standard deviation of three technical replicates. Similar results were obtained from three biological replicates.

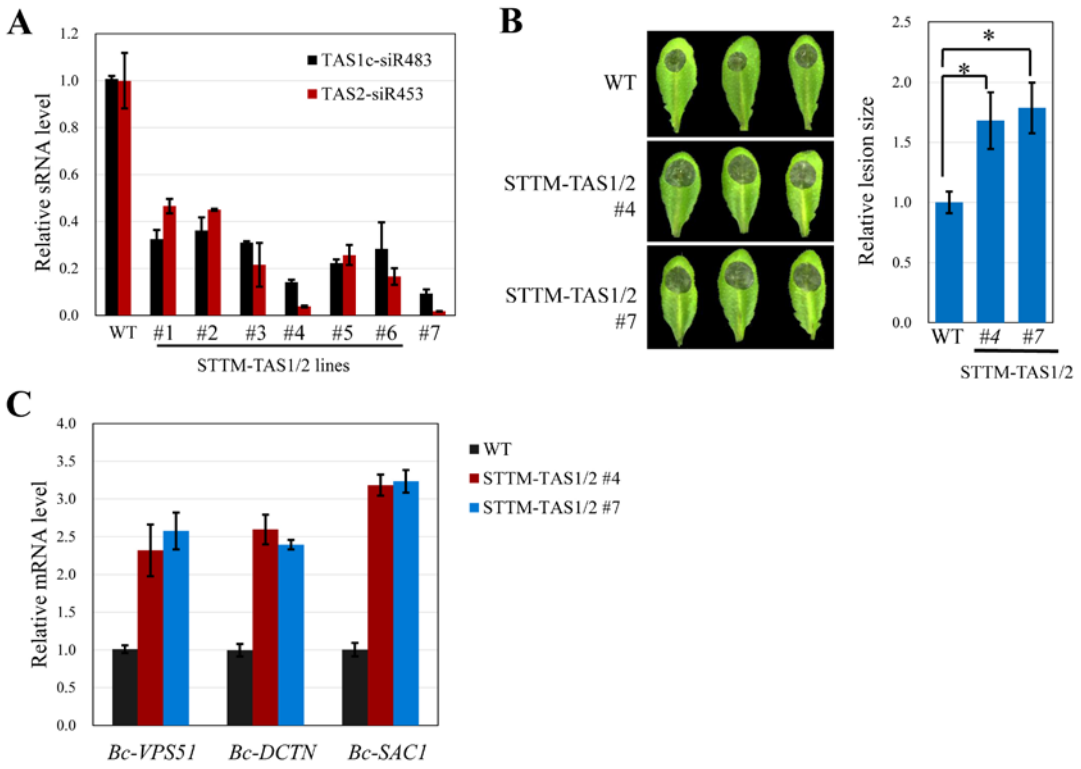

Fig. S15. Transgenic STTM lines that knocking down both TAS1c-siR483 and TAS2-siR453 show enhanced susceptibility to *B. cinerea* as compared with wild type. (A) Expression of TAS1c-siR483 and TAS2-siR453 in STTM transgenic plants (STTM-TAS1/2) was examined by quantitative RT-PCR measurements. The expression level of TAS1c-siR483 and TAS2-siR453 in wild-type plants was set as 1. The *At-Actin* gene was used as an internal control. Two lines (#4 and #7) with low tasiRNA expression were selected for further experiments. (B) The STTM-TAS1/2 lines are more susceptible to *B. cinerea* infection. Relative lesion sizes were measured at 2.5 dpi using ImageJ. Error bars indicate the standard deviation of more than 10 leaves. Asterisks indicate significant differences (ANOVA Dunnett's multiple comparisons test, $P<0.01$). (C) Quantitative RT-PCR results showed the expression level of *Bc-VPS51*, *Bc-DCTN1* and *Bc-SAC1* elevated in *B. cinerea* from infected STTM-TAS1/2 plants compared with the wild type. The *Actin* gene of *B. cinerea* was used as an internal control. Error bars indicate the standard deviation of three technical replicates. Similar results were obtained from three biological replicates.

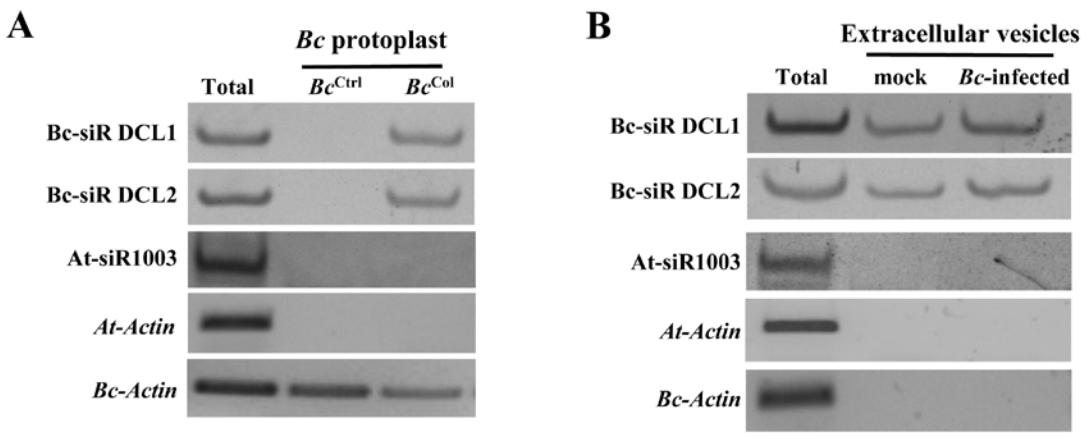

Fig. S16. Plants also use extracellular vesicles to deliver transgene-derived sRNAs into fungal cells. (A) Transgene-derived *Bc-DCL1*-sRNAs and *Bc-DCL2*-sRNAs were detected by sRNA RT-PCR in purified *B. cinerea* protoplasts (Bc^{Col}) from *B. cinerea*-infected *Bc-DCL1/2*-RNAi plants but not in the mock-treated plants mixed with *B. cinerea* mycelium before protoplast preparation(Bc^{Ctrl}). (B) Transgene-derived *Bc-DCL1*-sRNAs and *Bc-DCL2*-sRNAs were detected in extracellular vesicles from *B. cinerea*-infected *Arabidopsis Bc-DCL1/2*-RNAi plants. *Arabidopsis* At-siR1003 and *B. cinerea Actin* genes were used as controls. The 'total' lane indicates total RNA extracts from whole leaves.

Supplementary tables

Table S1 (separate file)

This file contains a list of *Arabidopsis* endogenous sRNAs present in the sRNA libraries of purified *B. cinerea* protoplasts from infected tissue. The normalized reads of these sRNAs in the extracellular vesicles and total sRNA libraries are compared.

Table S2 (separate file)

This table contains the list of the top 100 most abundant *Arabidopsis* sRNAs present in total sRNA libraries. The normalized reads of these sRNAs in *B. cinerea* protoplast and extracellular vesicle sRNA libraries are compared.

Table S3 (separate file)

This table contains the list of sRNAs from purified *B.cinerea* protoplast sRNA libraries that are not present in the top 100 most abundant sRNAs from total sRNA libraries. The normalized reads of these sRNAs in the total sRNA libraries and extracellular vesicle sRNA libraries are compared.

Table S4 (separate file)

This file contains a list of *Arabidopsis* sRNAs present in extracellular vesicles. The normalized reads of these sRNAs in the *B. cinerea* protoplast and total sRNA libraries are compared.

Table S5 (separate file)

This table contains the list of *B. cinerea* genes targeted by *Arabidopsis* endogenous sRNAs that were detected in purified *B. cinerea* protoplasts.

Table S6 (separate file)

This table contains the list of primers used in this study.

References and Notes

1. D. Baulcombe, RNA silencing in plants. *Nature* **431**, 356–363 (2004). doi:10.1038/nature02874 Medline

2. M. Mittelbrunn, F. Sánchez-Madrid, Intercellular communication: Diverse structures for exchange of genetic information. *Nat. Rev. Mol. Cell Biol.* **13**, 328–335 (2012). doi:10.1038/nrm3335 Medline

3. A. Molnar, C. W. Melnyk, A. Bassett, T. J. Hardcastle, R. Dunn, D. C. Baulcombe, Small silencing RNAs in plants are mobile and direct epigenetic modification in recipient cells. *Science* **328**, 872–875 (2010). doi:10.1126/science.1187959 Medline

4. A. Weiberg, M. Bellinger, H. Jin, Conversations between kingdoms: Small RNAs. *Curr. Opin. Biotechnol.* **32**, 207–215 (2015). doi:10.1016/j.copbio.2014.12.025 Medline

5. M. Wang, N. Thomas, H. Jin, Cross-kingdom RNA trafficking and environmental RNAi for powerful innovative pre- and post-harvest plant protection. *Curr. Opin. Plant Biol.* **38**, 133–141 (2017). doi:10.1016/j.pbi.2017.05.003 Medline

6. A. Weiberg, M. Wang, F.-M. Lin, H. Zhao, Z. Zhang, I. Kaloshian, H.-D. Huang, H. Jin, Fungal small RNAs suppress plant immunity by hijacking host RNA interference pathways. *Science* **342**, 118–123 (2013). doi:10.1126/science.1239705 Medline

7. A. H. Buck, G. Coakley, F. Simbari, H. J. McSorley, J. F. Quintana, T. Le Bihan, S. Kumar, C. Abreu-Goodger, M. Lear, Y. Harcus, A. Ceroni, S. A. Babayan, M. Blaxter, A. Ivens, R. M. Maizels, Exosomes secreted by nematode parasites transfer small RNAs to mammalian cells and modulate innate immunity. *Nat. Commun.* **5**, 5488 (2014). doi:10.1038/ncomms6488 Medline

8. M. Wang, A. Weiberg, F.-M. Lin, B. P. H. J. Thomma, H.-D. Huang, H. Jin, Bidirectional cross-kingdom RNAi and fungal uptake of external RNAs confer plant protection. *Nat. Plants* **2**, 16151 (2016). doi:10.1038/nplants.2016.151 Medline

9. S. Shahid, G. Kim, N. R. Johnson, E. Wafula, F. Wang, C. Coruh, V. Bernal-Galeano, T. Phifer, C. W. dePamphilis, J. H. Westwood, M. J. Axtell, MicroRNAs from the parasitic plant Cuscuta campestris target host messenger RNAs. *Nature* **553**, 82–85 (2018). doi:10.1038/nature25027 Medline

10. T. Zhang, Y.-L. Zhao, J.-H. Zhao, S. Wang, Y. Jin, Z.-Q. Chen, Y.-Y. Fang, C.-L. Hua, S.-W. Ding, H.-S. Guo, Cotton plants export microRNAs to inhibit virulence gene expression in a fungal pathogen. *Nat. Plants* **2**, 16153 (2016). doi:10.1038/nplants.2016.153 Medline

11. M. Wang, A. Weiberg, E. Dellota Jr., D. Yamane, H. Jin, Botrytis small RNA *Bc*-siR37 suppresses plant defense genes by cross-kingdom RNAi. *RNA Biol.* **14**, 421–428 (2017). doi:10.1080/15476286.2017.1291112 Medline

12. A. Weiberg, H. Jin, Small RNAs—the secret agents in the plant-pathogen interactions. *Curr. Opin. Plant Biol.* **26**, 87–94 (2015). doi:10.1016/j.pbi.2015.05.033 Medline

13. M. Colombo, G. Raposo, C. Théry, Biogenesis, secretion, and intercellular interactions of exosomes and other extracellular vesicles. *Annu. Rev. Cell Dev. Biol.* **30**, 255–289 (2014). doi:10.1146/annurev-cellbio-101512-122326 Medline

14. H. Valadi, K. Ekström, A. Bossios, M. Sjöstrand, J. J. Lee, J. O. Lötvall, Exosome-mediated transfer of mRNAs and microRNAs is a novel mechanism of genetic exchange between cells. *Nat. Cell Biol.* **9**, 654–659 (2007). doi:10.1038/ncb1596 Medline

15. M. Mittelbrunn, C. Gutiérrez-Vázquez, C. Villarroya-Beltri, S. González, F. Sánchez-Cabo, M. Á. González, A. Bernad, F. Sánchez-Madrid, Unidirectional transfer of microRNA-loaded exosomes from T cells to antigen-presenting cells. *Nat. Commun.* **2**, 282 (2011). doi:10.1038/ncomms1285 Medline

16. S. Mathivanan, H. Ji, R. J. Simpson, Exosomes: Extracellular organelles important in intercellular communication. *J. Proteomics* **73**, 1907–1920 (2010). doi:10.1016/j.jprot.2010.06.006 Medline

17. L. C. Boavida, P. Qin, M. Broz, J. D. Becker, S. McCormick, Arabidopsis tetraspanins are confined to discrete expression domains and cell types in reproductive tissues and form homo- and heterodimers when expressed in yeast. *Plant Physiol.* **163**, 696–712 (2013). doi:10.1104/pp.113.216598 Medline

18. S. Ferrari, R. Galletti, C. Denoux, G. De Lorenzo, F. M. Ausubel, J. Dewdney, Resistance to Botrytis cinerea induced in Arabidopsis by elicitors is independent of salicylic acid, ethylene, or jasmonate signaling but requires PHYTOALEXIN DEFICIENT3. *Plant Physiol.* **144**, 367–379 (2007). doi:10.1104/pp.107.095596 Medline

19. M. Ostrowski, N. B. Carmo, S. Krumeich, I. Fanget, G. Raposo, A. Savina, C. F. Moita, K. Schauer, A. N. Hume, R. P. Freitas, B. Goud, P. Benaroch, N. Hacohen, M. Fukuda, C. Desnos, M. C. Seabra, F. Darchen, S. Amigorena, L. F. Moita, C. Thery, Rab27a and Rab27b control different steps of the exosome secretion pathway. *Nat. Cell Biol.* **12**, 19–30, 1–13 (2010). doi:10.1038/ncb2000 Medline

20. K. Ebine, M. Fujimoto, Y. Okatani, T. Nishiyama, T. Goh, E. Ito, T. Dainobu, A. Nishitani, T. Uemura, M. H. Sato, H. Thordal-Christensen, N. Tsutsumi, A. Nakano, T. Ueda, A membrane trafficking pathway regulated by the plant-specific RAB GTPase ARA6. *Nat. Cell Biol.* **13**, 853–859 (2011). doi:10.1038/ncb2270 Medline

21. S. Levy, T. Shoham, The tetraspanin web modulates immune-signalling complexes. *Nat. Rev. Immunol.* **5**, 136–148 (2005). doi:10.1038/nri1548 Medline

22. Z. Xie, E. Allen, A. Wilken, J. C. Carrington, DICER-LIKE 4 functions in trans-acting small interfering RNA biogenesis and vegetative phase change in Arabidopsis thaliana. *Proc. Natl. Acad. Sci. U.S.A.* **102**, 12984–12989 (2005). doi:10.1073/pnas.0506426102 Medline

23. J. S. Bonifacino, A. Hierro, Transport according to GARP: Receiving retrograde cargo at the trans-Golgi network. *Trends Cell Biol.* **21**, 159–167 (2011). doi:10.1016/j.tcb.2010.11.003 Medline

24. Y. Liu, R. Mittal, N. V. Solis, N. V. Prasadarao, S. G. Filler, Mechanisms of Candida albicans trafficking to the brain. *PLOS Pathog.* **7**, e1002305 (2011). doi:10.1371/journal.ppat.1002305 Medline

25. M. O. Steinmetz, A. Akhmanova, Capturing protein tails by CAP-Gly domains. *Trends Biochem. Sci.* **33**, 535–545 (2008). doi:10.1016/j.tibs.2008.08.006 Medline

26. Y. Liu, V. A. Bankaitis, Phosphoinositide phosphatases in cell biology and disease. *Prog. Lipid Res.* **49**, 201–217 (2010). doi:10.1016/j.plipres.2009.12.001 Medline

27. C. Catalanotto, G. Azzalin, G. Macino, C. Cogoni, Involvement of small RNAs and role of the qde genes in the gene silencing pathway in Neurospora. *Genes Dev.* **16**, 790–795 (2002). doi:10.1101/gad.222402 Medline

28. G. LaMonte, N. Philip, J. Reardon, J. R. Lacsina, W. Majoros, L. Chapman, C. D. Thornburg, M. J. Telen, U. Ohler, C. V. Nicchitta, T. Haystead, J.-T. Chi, Translocation of sickle cell erythrocyte microRNAs into Plasmodium falciparum inhibits parasite translation and contributes to malaria resistance. *Cell Host Microbe* **12**, 187–199 (2012). doi:10.1016/j.chom.2012.06.007 Medline

29. I. R. Henderson, X. Zhang, C. Lu, L. Johnson, B. C. Meyers, P. J. Green, S. E. Jacobsen, Dissecting Arabidopsis thaliana DICER function in small RNA processing, gene silencing and DNA methylation patterning. *Nat. Genet.* **38**, 721–725 (2006). doi:10.1038/ng1804 Medline

30. M. Grebe, J. Xu, W. Möbius, T. Ueda, A. Nakano, H. J. Geuze, M. B. Rook, B. Scheres, Arabidopsis sterol endocytosis involves actin-mediated trafficking via ARA6-positive early endosomes. *Curr. Biol.* **13**, 1378–1387 (2003). doi:10.1016/S0960-9822(03)00538-4 Medline

31. Z. Xie, L. K. Johansen, A. M. Gustafson, K. D. Kasschau, A. D. Lellis, D. Zilberman, S. E. Jacobsen, J. C. Carrington, Genetic and functional diversification of small RNA pathways in plants. *PLOS Biol.* **2**, E104 (2004). doi:10.1371/journal.pbio.0020104 Medline

32. F. Fauser, S. Schiml, H. Puchta, Both CRISPR/Cas-based nucleases and nickases can be used efficiently for genome engineering in *Arabidopsis thaliana*. *Plant J.* **79**, 348–359 (2014). doi:10.1111/tpj.12554 Medline

33. R. Schwab, S. Ossowski, M. Riester, N. Warthmann, D. Weigel, Highly specific gene silencing by artificial microRNAs in Arabidopsis. *Plant Cell* **18**, 1121–1133 (2006). doi:10.1105/tpc.105.039834 Medline

34. G. Tang, J. Yan, Y. Gu, M. Qiao, R. Fan, Y. Mao, X. Tang, Construction of short tandem target mimic (STTM) to block the functions of plant and animal microRNAs. *Methods* **58**, 118–125 (2012). doi:10.1016/j.ymeth.2012.10.006 Medline

35. D. Niu, J. Xia, C. Jiang, B. Qi, X. Ling, S. Lin, W. Zhang, J. Guo, H. Jin, H. Zhao, *Bacillus cereus* AR156 primes induced systemic resistance by suppressing miR825/825* and activating defense-related genes in *Arabidopsis*. *J. Integr. Plant Biol.* **58**, 426–439 (2016). doi:10.1111/jipb.12446 Medline

36. Y. Yun, Z. Liu, J. Zhang, W.-B. Shim, Y. Chen, Z. Ma, The MAPKK FgMkk1 of *Fusarium graminearum* regulates vegetative differentiation, multiple stress response, and virulence via the cell wall integrity and high-osmolarity glycerol signaling pathways. *Environ. Microbiol.* **16**, 2023–2037 (2014). doi:10.1111/1462-2920.12334 Medline

37. D. J. Cosgrove, Growth of the plant cell wall. *Nat. Rev. Mol. Cell Biol.* **6**, 850–861 (2005). doi:10.1038/nrm1746 Medline

38. S. M. Bowman, S. J. Free, The structure and synthesis of the fungal cell wall. *BioEssays* **28**, 799–808 (2006). doi:10.1002/bies.20441 Medline

39. S. D. Yoo, Y. H. Cho, J. Sheen, Arabidopsis mesophyll protoplasts: A versatile cell system for transient gene expression analysis. *Nat. Protoc.* **2**, 1565–1572 (2007). doi:10.1038/nprot.2007.199 Medline

40. B. D. Rutter, R. W. Innes, Extracellular Vesicles Isolated from the Leaf Apoplast Carry Stress-Response Proteins. *Plant Physiol.* **173**, 728–741 (2017). doi:10.1104/pp.16.01253 Medline

41. M. Regente, G. Corti-Monzón, A. M. Maldonado, M. Pinedo, J. Jorrín, L. de la Canal, Vesicular fractions of sunflower apoplastic fluids are associated with potential exosome marker proteins. *FEBS Lett.* **583**, 3363–3366 (2009). doi:10.1016/j.febslet.2009.09.041 Medline

42. C. Thery, S. Amigorena, G. Raposo, A. Clayton, *Current protocols in cell biology* **Chapter 3**, Unit 3 22 (2006).

43. M. E. Nielsen, A. Feechan, H. Böhlenius, T. Ueda, H. Thordal-Christensen, Arabidopsis ARF-GTP exchange factor, GNOM, mediates transport required for innate immunity and focal accumulation of syntaxin PEN1. *Proc. Natl. Acad. Sci. U.S.A.* **109**, 11443–11448 (2012). doi:10.1073/pnas.1117596109 Medline